NeuroImage: Clinical 36 (2022) 103165

Contents lists available at ScienceDirect

NeuroImage: Clinical

journal homepage: www.elsevier.com/locate/ynicl

Perfusion heterogeneity of cerebral small vessel disease revealed via arterial spin labeling MRI and machine learning

Weizhao Lu [a,b], Chunyan Yu [b], Liru Wang [b], Feng Wang [a,*], Jianfeng Qiu [a,b,*]

[a] Department of Radiology, The Second Affiliated Hospital of Shandong First Medical University, Taian, China
[b] School of Radiology, Shandong First Medical University & Shandong Academy of Medical Sciences, Taian, China

ARTICLE INFO

Keywords:
Cerebral small vessel disease
Cerebral blood flow
Arterial spin labeling
White matter hyperintensity
Lacune
Machine learning

ABSTRACT

Cerebral small vessel disease (CSVD) is associated with altered cerebral perfusion. However, global and regional cerebral blood flow (CBF) are highly heterogeneous across CSVD patients. The aim of this study was to identify subtypes of CSVD with different CBF patterns using an advanced machine learning approach. 121 CSVD patients and 53 healthy controls received arterial spin label MRI, T1 structural MRI and clinical measurements. Regional CBF were used to identify distinct perfusion subtypes of CSVD via a semi-supervised machine learning algorithm. Statistical analyses were used to explore alterations in CBF, clinical measures, gray and white matter volume between healthy controls and different subtypes of CSVD. Correlation analysis was used to assess the association between clinical measures and altered CBF in each CSVD subtype. Three subtypes of CSVD with distinct CBF patterns were found. Subtype 1 showed decreased CBF in the temporal lobe and increased CBF in the parietal and occipital lobe. Subtype 2 exhibited decreased CBF in the right hemisphere of the brain, and increased CBF in the left cerebrum. Subtype 3 demonstrated decreased CBF in the posterior part of the brain, and increased CBF in anterior part of the brain. The three subtypes also differed significantly in gender ($p = 0.005$), the proportion of subjects with lacune ($p = 0.002$), with periventricular white matter hyperintensity ($p = 0.043$), and CSVD burden score ($p = 0.048$). In subtype 3, it was found that widespread decreased CBF was correlated with total CSVD burden score ($r = -0.324$, $p = 0.029$). Compared with healthy controls, the three CSVD subtypes also showed distinct volumetric patterns of white matter. The current results associate different subtypes with different clinical and imaging phenotypes, which can improve the understanding of brain perfusion alterations of CSVD and can facilitate precision diagnosis of CSVD.

1. Introduction

Cerebral small vessel disease (CSVD) is a widespread cerebrovascular disease which affects small arteries, arterioles, and capillaries of the brain (Li et al., 2018). Currently, the incidence of CSVD worldwide is as high as 3–8 %, with a rising trend in the aging population (Wardlaw et al., 2020). Risk factors of CSVD include aging, hypertension, and genetic variations (Li et al., 2018; Wardlaw et al., 2020). However, the pathogenesis of CSVD is still unclear so far (Cannistraro et al., 2019). Researchers have revealed that CSVD has close associations with cognitive impairment, stroke, dementia, and psychiatric disorders (Cannistraro et al., 2019; Salvadori et al., 2016).

Currently, the detection of CSVD mainly depends on MRI (Pantoni, 2010). The MRI markers of CSVD include lacune of presumed vascular origin, small subcortical infarct, white matter hyperintensity (WMH), enlarged perivascular space (EPVS), and cerebral microbleeds (CMBs) (Chen et al., 2019). Despite the existence of MRI markers in regional brain regions, CSVD is currently considered to be a global and dynamically changing disease across the entire brain (Shi and Wardlaw, 2016; Ter Telgte et al., 2018). CSVD can cause alterations of the overall brain structural network as manifested by decreased structural connectivity, reduced global efficiency (Tuladhar et al., 2017). CSVD can also result in disrupted local structural connections in the interhemispheric and prefrontal regions (Lawrence et al., 2014). In addition, reduced functional

Abbreviations: CSVD, cerebral small vessel disease; WMH, white matter hyperintensity; EPVS, enlarged perivascular space; CMB, cerebral microbleed; ASL, arterial spin labelling; CBF, cerebral blood flow.

* Corresponding authors at: No. 706 Taishan Street, The Second Affiliated Hospital of Shandong First Medical University, Taian 271000, China (F. Wang). No. 619 Changcheng Road, Shandong First Medical University & Shandong Academy of Medical Sciences, Taian 271000, China (J. Qiu).

E-mail addresses: 168973832@qq.com (F. Wang), jfqiu100@gmail.com (J. Qiu).

https://doi.org/10.1016/j.nicl.2022.103165
Received 13 April 2022; Received in revised form 9 August 2022; Accepted 22 August 2022

connectivity within the default-mode network, dorsal attention network, frontoparietal control network have been observed in patients with CSVD (Spreng et al., 2013). More importantly, WMHs and subcortical infarcts of CSVD are accompanied by reduced brain perfusion (Hillis et al., 2002; Tullberg et al., 2004). Previous studies have shown that decreased global and regional cerebral blood flow (CBF) are associated with disease severity in patients with CSVD (Yu et al., 2020; Shi et al., 2016).

However, alterations of CBF in CSVD patients were not consistent among previous studies (Shi et al., 2016; Stewart et al., 2021). In some cross-sectional studies, lower CBF was significantly related to CSVD total burden (Yu et al., 2020; Shi et al., 2016). In other studies, no such relationship was found (Shi et al., 2016; Kuwabara et al., 1996). Furthermore, in a previous study by our group, we have found variances of regional CBF in CSVD patients (Yu et al., 2020). Therefore, it was hypothesized that CSVD is associated with disparities and heterogeneity in brain perfusions. Heterogeneity through discriminative analysis (HYDRA), a recently-proposed semi-supervised machine learning method which has been successfully used in the subtyping of Alzheimer's disease and schizophrenia (Varol et al., 2017; Chand et al., 2020), was applied to characterize different patterns of CBF in CSVD patients. Associations between CBF and clinical measures were assessed in different CSVD subtypes. In addition, gray and white matter volumetric differences were investigated among CSVD subtypes to test the rationality of the subtyping.

2. Methods

2.1. Subject enrollment

This study was approved by the Institution Review Board according to the principles of the Declaration of Helsinki. Written informed consent was obtained from all participants or their legally acceptable representatives.

232 Subjects were recruited by the affiliated hospital of our university between October 2018 and January 2021. CSVD patients were included according to the following inclusion criteria (Yu et al., 2020): (1) evidence of CSVD defined as small vessel occlusion stroke (lacunar stroke syndrome) with symptoms lasting over 24 h, occurring $>$ 6 months prior to the visit (Binnie et al., 2022); (2) blood biochemistry indexes, liver and kidney function indexes all in normal ranges; (3) one or more MRI markers of CSVD defined as WMH, lacune, CMBs, and EPVS based on clinical-routine brain MRI scan (the brain MRI scan parameters are given in the Supplementary Text). Exclusion criteria were: (1) brain tumor or other systemic malignant tumors; (2) history of traumatic brain injury; (3) acute massive cerebral infarction (diameter $>$ 2 cm) or magnetic resonance angiography showing artery stenosis; (4) abnormal cerebral vascular development, such as posterior cerebral artery of the embryonic brain; (4) mental disorders and consciousness disorders; (5) atrial fibrillation, acute ischemic stroke caused by cardiogenic embolism; (6) other disorders that affect brain perfusion; (7) stroke or transient ischemic attack within 6 months; (8) MRI contradictions.

Healthy controls were included with the following criteria: (1) no clinical evidence of CSVD, and CSVD total burden score of 0 evaluated by two experienced radiologists based on the clinical routine MRI scans (Supplementary Text); (2) no brain tumors or other systemic malignant tumors, no history of brain injuries, no mental disorders or consciousness disorders; (3) no disorders that affect brain perfusion; (4) no MRI contradictions.

At last, 174 subjects including 121 CSVD patients and 53 healthy controls were enrolled for further analysis (Supplementary Figure S1). The 174 subjects received comprehensive clinical examinations.

2.2. MRI acquisition and clinical examination

A 3.0 T MRI (GE Discovery MR 750) with an 8-channel head coil was used. Perfusion images were obtained using a pseudo continuous arterial spin labeling (ASL) approach with a 3D fast spin-echo sequence: 14 sampling points on 8 spirals, field of view = 220 × 220 mm^2; reconstructed matrix = 128 × 128, time of repetition (TR) = 4781 ms, echo time (TE) = 11.1 ms, number of excitations = 3.0, slice thickness = 3.0 mm, labeling plane was positioned at the base of the cerebellum with labeling duration = 1500 ms and post labeling delay = 1525 ms, 45 volumes, and an acquisition time of 4 min 37 s. 3D BRAVO sequence was used to collect T1 images for assessing brain parenchymal volume. The scan parameters were: TR = 8.2 ms, TE = 3.2 ms, flip angle = 12°, FOV = 240 × 240 mm^2, acquisition matrix = 256 × 256, slice thickness = 1.2 mm with 120 sagittal slices covering the whole brain, and an acquisition time of 3 min 27 s.

CSVD markers including lacunes, WMH, CMBs, and EPVS were evaluated according to the Standards for Reporting Vascular Changes on Neuroimaging (STRIVE) criteria by two experienced radiologists. Negotiations were conducted if there were disagreements. The total CSVD burden score and scores for the four MRI markers were rated (Supplementary Table S1 lists the score criterion, Supplementary Figure S2-S6 show MRI images of subjects with different total CSVD burden score).

In addition, binary variables (whether or not) of hypertension, hyperlipidemia, diabetes, coronary heart disease, smoking cigarette and drinking alcohol were obtained from all the enrolled subjects. Blood biochemical indexes, including concentrations of low-density lipoprotein (LDL), high-density lipoprotein (HDL), triglyceride, glutamic acid, homocysteine, free fatty acid, apolipoprotein A, apolipoprotein B, and total cholesterol were measured.

2.3. ASL data preprocessing

Image preprocessing included the following steps: (1) quantitative CBF map was calculated from ASL images using the Functool software (Version 9.4.05) in the MRI server with necessary corrections including partial volume effect correction; (2) quality check was performed by an experienced radiologist to exclude low-quality data; (3) a two-step normalization of CBF map was performed using SPM12: Firstly, T1-weighted image was co-registered to CBF map using affine transformation, followed by a nonlinear registration of the co-registered T1-weighted image to the Montreal Neurological Institute (MNI) standard template. Finally, the deformation field of the nonlinear registration was applied to the CBF map; (4) after normalization, the CBF map was smoothed with a 6 mm full width at half maximum (FWHM) isotropic Gaussian kernel; (5) the CBF map was standardized using the following formula.

$$sCBF(i) = \frac{CBF(i)}{CBF_{global\_mean}}$$

where sCBF(i) is the value of the ith voxel in the standardized CBF map of one subject, CBF(i) is the value of the ith voxel in the CBF map, and CBF_{global_mean} is the mean CBF value across the brain of the subject.

2.4. Subtype of CSVD and reproducibility analysis

In this study, HYDRA was applied to identify subtypes of CSVD patients with distinct brain perfusion. The features of HYDRA were selected as regional CBF based on the parcellation of Brainnetome atlas (Fan et al., 2016). HYDRA compared CSVD patients with healthy controls to identify the subtypes within the CSVD patients. The process of the algorithm included the following steps: Firstly, the subjects were split by a 10-fold cross validation strategy. In the training set, a linear maximum margin classifier was introduced to calculate the distance from the feature point of each CSVD subject to each hyperplane, then CSVD patients were assigned to the hyperplane closest to themselves. In this way, CSVD patients in the training set were divided into K clusters. Finally, each CSVD subject participated in 9 clustering processes and

obtained 9 same or different clustering labels. The consensus clustering was applied to generate the final cluster label of each CSVD patients based on a cooccurrence matrix generated from the labels of the 9 clustering processes. In addition, HYDRA quantified the clustering stability among the clustering results in the 10-folds cross-validation by the adjusted rand index (ARI) (Chand et al., 2020).

In order to evaluate the effect of regional CBF feature definition on the final clustering result, we also used the Brodmann area and anatomical automatic labeling (AAL) atlas to define regional CBF features for HYDRA to perform the clustering of CSVD patients (Zilles and Amunts, 2010; Rolls et al., 2020). In addition, clustering reproducibility was analyzed using the permutation test. For each permutation, a null distribution was configured with 11 healthy controls and 42 pseudo CSVD patients (the same ratio of the actual healthy controls and CSVD patients). The healthy controls and pseudo patients were randomly selected from the control group. Then, HYDRA was applied on the null distribution. The actual distribution was configured with 11 healthy controls and 42 real CSVD patients randomly selected from the healthy controls and CSVD patients, and HYDRA analysis was also performed to the actual distribution. The permutation step was repeated 10 times. Finally, the ARIs obtained from the actual distributions were compared with those obtained from the null distributions to evaluate the reproducibility of the clustering.

2.5. Statistical analysis

Voxel-wise CBF analysis was conducted to explore CBF alterations between different subtypes of CSVD patients and healthy controls. General linear model was used for voxel-wise CBF analysis, age and gender were taken as nuisance covariates. For multiple comparison, permutation test (10000 times) with threshold-free cluster enhancement (TFCE) was used to control false positives. We also reported effect size (ES) calculated by Cohen's *d* in voxel-wise CBF analysis.

For statistical analysis of demographic and clinical information between CSVD patients and healthy controls, parametric tests were used on continuous data which followed normal distributions, and non-parametric tests were used on nominal or ordinal variables. Specifically, analysis of variance (ANOVA) was used to assess differences in age, blood biochemical indexes, with Bonferroni approach used for post-hoc multiple comparison corrections. Chi-square test was used to assess differences in gender, the proportion of subjects with hypertension, diabetes, hyperlipidemia, coronary heart disease, smoking cigarette and drinking alcohol. Chi-square test was also used for pairwise comparisons.

Among different subtypes of CSVD, chi-square test was used to assess differences in the proportion of patients with MRI markers including lacune, white matter lesions, WMH, EPVS and CMBs. Chi-square test was also used for pairwise comparisons. Kruskal-Wallis test was used to assess differences in total scores of WMH, EPVS and CMBs, and total CSVD burden score. Mann-Whitney *U* test was used for every pairwise comparisons.

While each CSVD subtype exhibited both increased and decreased CBF compared with healthy controls, we extracted the mean CBF values from the brain regions with increased and decreased CBF. Pearson correlation analysis was applied between the mean CBFs from the brain regions with increased and decreased CBF to investigate possible compensatory effects in cerebral perfusion. In addition, within each subtype, associations between CBF and total CSVD burden score were assessed by Pearson correlation analysis.

2.6. T1 structural image processing and volumetric analysis

Volumetric analysis of gray and white matter was performed to test whether the CSVD subtypes differed in gray matter and white matter volumes. CAT12 was applied for the preprocessing of T1 structural MRI data with the following steps: (1) normalization of T1 image into the MNI space and the voxel size was resampled into $1.5 \times 1.5 \times 1.5\ mm^3$; (2) segmentation of the normalized images into gray matter, white matter and CSF; (3) modulation to convert the voxel values from tissue concentration (density) to volume; (4) calculation of the volume value based on the ROI from gray matter, white matter and CSF; (5) smoothing with a 6 mm FWHM isotropic Gaussian kernel. General linear model was used for voxel-wise gray matter and white matter analysis between healthy controls and CSVD subtypes, age and gender were taken as nuisance covariates.

3. Results

3.1. Three reproducible subtypes of CSVD

HYDRA was applied to the CBF of different brain regions according to the brain parcellation by Brainnetome atlas with the resolution K ranging from 2 to 10 clusters. ARI was calculated as the measure of reproducibility. Clustering results demonstrated that $K = 3$ achieved the maximum reproducibility (Fig. 1a). In order to evaluate the effect of feature definition, we also used Brodmann atlas and AAL atlas to parcellate the brain and obtain regional CBF features for HYDRA analysis. The results were consistent with the original experiment (Fig. 1a), which indicated CSVD patients could be partitioned into 3 subtypes regardless of feature definition.

To evaluate the stability and reproducibility of the subtyping, the distribution of CSVD patients were compared with a null distribution generated by permutation tests. The results are shown in Fig. 1b. The ARIs at $K = 2$, 3 and 10 from CSVD distributions were higher than those from null distributions ($p < 0.05$). Given the subtyping and reproducibility results, subsequent analyses focused on three subtypes.

3.2. Demographic and clinical information

Demographic and clinical information for healthy controls and three CSVD subtypes are shown in Table 1. There were significant differences in age ($p < 0.001$), gender ($p = 0.006$), the proportion of subjects with hypertension ($p = 0.009$), smoking ($p = 0.018$) and drinking habits ($p = 0.009$) among healthy controls and the three CSVD subtypes. Post-hoc multiple comparisons revealed that healthy subjects were younger in age, and exhibited lower proportions of subjects with hypertension, smoking and drinking habits compared with CSVD subtypes. In addition, differences in gender ratios were observed between subtype 1 and subtype 2 ($\chi^2 = 5.031$, $p = 0.025$), between subtype 2 and subtype 3 ($\chi^2 = 9.705$, $p = 0.002$).

3.3. Voxel-wise CBF map and MRI markers of CSVD subtypes

The three subtypes of CSVD patients showed differences in their voxel-wise patterns of CBF compared with healthy controls (Fig. 2), the three subtypes of CSVD patients also demonstrated distinct perfusion patterns among each other (Supplementary Figure S7). Compared with healthy controls ($n = 53$), subtype 1 ($n = 39$) exhibited decreased CBF in the left temporal lobe (inferior, middle and superior temporal gyrus) ($T = 5.6864$, $p < 0.05$ corrected by permutation test with TFCE, absolute $ES = 0.37$), subtype 1 also exhibited increased CBF in the right parietal lobe (superior parietal gyrus), right precuneus, right postcentral gyrus, and right occipital lobe (middle and superior occipital gyrus) ($T = 6.6741$, $p < 0.05$ corrected by permutation test with TFCE, absolute $ES = 0.51$). In terms of demographic and clinical information, CSVD subtype 1 were older in age than healthy controls ($T = 4.442$, $p < 0.001$), and exhibited higher possibility of smoking cigarette ($\chi^2 = 5.349$, $p = 0.021$) and drinking alcohol ($\chi^2 = 6.543$, $p = 0.011$) compared with healthy controls.

Compared with healthy subjects ($n = 53$), subtype 2 ($n = 41$) showed decreased CBF mainly in the right hemisphere of the brain, including the frontal, temporal, parietal and part of occipital lobe ($T = 7.8752$, $p <$

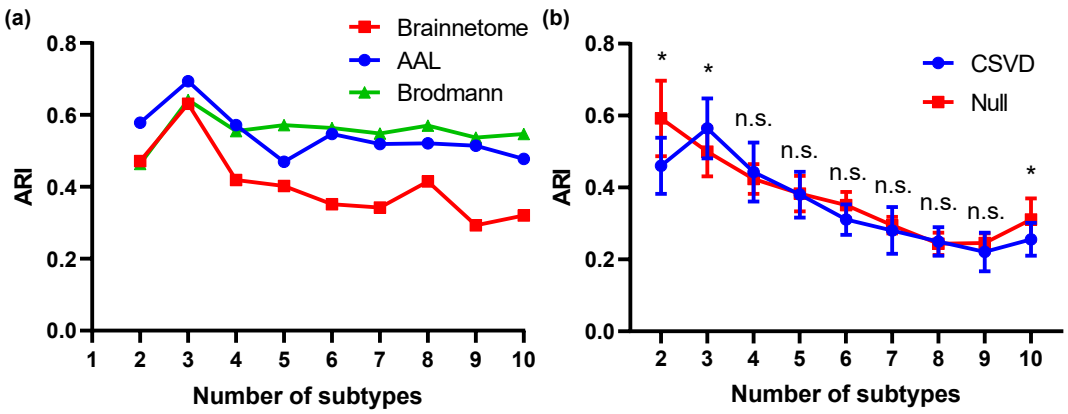

Fig. 1. Subtyping of CSVD based on regional CBF. (a) ARI obtained for different subtypes (*K*) via the original CBF features (defined by regional CBF according to the Brainnetome atlas) and two other CBF feature definition strategies (regional CBF defined by the Brodmann atlas and AAL atlas respectively). (b) Statistical significance of ARI obtained for different subtypes (*K*) in comparison with the null distribution obtained from random permutations. Abbreviations: n.s., not significant.

Table 1
Demographic and clinical information for the enrolled subjects.

		HC (n = 53)	CSVD1 (n = 39)	CSVD2 (n = 41)	CSVD3 (n = 41)	Statistics	*p*
Age		57.13 ± 9.29	65.43 ± 8.23	64.75 ± 8.38	61.80 ± 9.62	F = 8.544	**<0.001**†
Gender		25 M/28F	25 M/14F	16 M/25F	30 M/11F	χ^2 = 12.323	**0.006**‡
Hypertension		21Y/32 N	19Y/20 N	28Y/13 N	28Y/13 N	χ^2 = 11.546	**0.009**§
Diabetes		9Y/44 N	10Y/29 N	13Y/28 N	8Y/33 N	χ^2 = 3.276	0.351
Hyperlipemia		13Y/40 N	6Y/33 N	15Y/26 N	9Y/32 N	χ^2 = 5.099	0.165
Coronary heart disease		10Y/43 N	11Y/28 N	10Y/31 N	13Y/28 N	χ^2 = 2.244	0.523
Smoking		7Y/46 N	13Y/26 N	11Y/30 N	17Y/24 N	χ^2 = 10.094	**0.018**‖
Drinking		8Y/45 N	15Y/24 N	14Y/27 N	19Y/22 N	χ^2 = 11.634	**0.009**¶
Blood biochemical indexes*	LDL (mmol/L)	2.65 ± 0.70	2.77 ± 0.62	2.58 ± 0.61	2.74 ± 0.70	F = 0.398	0.755
	HDL (mmol/L)	1.23 ± 0.26	1.36 ± 0.31	1.43 ± 0.37	1.42 ± 0.59	F = 1.654	0.181
	TG (mmol/L)	1.64 ± 1.09	1.52 ± 0.72	1.28 ± 0.75	2.01 ± 1.97	F = 1.535	0.209
	GLU (mmol/L)	5.92 ± 3.24	5.06 ± 1.24	6.09 ± 2.40	5.98 ± 1.79	F = 0.989	0.401
	HCY (μmol/L)	13.80 ± 4.85	14.13 ± 6.55	16.61 ± 6.56	18.67 ± 10.82	F = 2.530	0.062
	FFA (mmol/L)	0.54 ± 0.26	0.46 ± 0.22	0.59 ± 0.27	0.57 ± 0.19	F = 1.346	0.264
	APOA (g/L)	1.22 ± 0.18	1.27 ± 0.24	1.21 ± 0.23	1.35 ± 0.34	F = 1.821	0.148
	APOB (g/L)	0.91 ± 0.23	1.01 ± 0.19	0.81 ± 0.28	0.97 ± 0.15	F = 2.100	0.111
	TC (mmol/L)	4.46 ± 0.99	5.09 ± 0.85	4.43 ± 1.30	5.00 ± 0.87	F = 1.736	0.171

† HC vs CSVD1, $p < 0.001$; HC vs CSVD2, $p < 0.001$.
‡ HC vs CSVD3, $\chi^2 = 6.438$, $p = 0.011$; CSVD1 vs CSVD2, $\chi^2 = 5.031$, $p = 0.025$; CSVD2 vs CSVD3, $p = 0.011$.
§ HC vs CSVD2, $\chi^2 = 7.614$, $p = 0.006$; HC vs CSVD3, $\chi^2 = 7.614$, $p = 0.006$.
‖HC vs CSVD1, $\chi^2 = 5.349$, $p = 0.021$; HC vs CSVD3, $\chi^2 = 9.707$, $p = 0.002$.
¶HC vs CSVD1, $\chi2 = 6.543$, $p = 0.011$; HC vs CSVD2, $\chi2 = 4.681$, $p = 0.031$; HC vs CSVD3, $\chi2 = 11.025$, $p = 0.001$.
* Normal range: LDL (2.07–3.3 mmol/L), HDL (1.03–1.85 mmol/L), TG (0.58–1.88 mmol/L), GLU (0–58 mmol/L), HCY (6–17 μmol/L), FFA (0.3 ~ 0.9 mmol/L), APOA (<1.6 g/L), APOB (<1.2 g/L), TC (2.33–5.69 mmol/L).
* Number of subjects with blood biochemical indexes. LDL: HC (n = 38), CSVD1 (n = 20), CSVD2 (n = 25), CSVD3 (n = 28); HDL, HC (n = 38), CSVD1 (n = 20), CSVD2 (n = 25), CSVD3 (n = 28); TG: HC (n = 38), CSVD1 (n = 22), CSVD2 (n = 26), CSVD3 (n = 29); GLU: HC (n = 37), CSVD1 (n = 22), CSVD2 (n = 25), CSVD3 (n = 29); HCY: HC (n = 34), CSVD1 (n = 17), CSVD2 (n = 23), CSVD3 (n = 26); FFA: HC (n = 34), CSVD1 (n = 18), CSVD2 (n = 24), CSVD3 (n = 27); APOA: HC (n = 34), CSVD1 (n = 18), CSVD2 (n = 24), CSVD3 (n = 28); APOB: HC (n = 13), CSVD1 (n = 9), CSVD2 (n = 22), CSVD3 (n = 15); TC: HC (n = 13), CSVD1 (n = 7), CSVD2 (n = 21), CSVD3 (n = 14).
Abbreviations: HC, healthy controls; CSVD1, CSVD subtype 1; CSVD2, CSVD subtype 2; CSVD3, CSVD subtype 3; M, male; F, female; Y, yes; N, no; LDL, low-density lipoprotein; HDL, high-density lipoprotein; TG, triglyceride; GLU, glutamic acid; HCY, homocysteine; FFA, free fatty acid; APOA, apolipoprotein A; APOB, apolipoprotein B; TC, total cholesterol.

0.05 corrected by permutation test with TFCE, absolute ES = 0.69). Subtype 2 also showed increased CBF prominently in the left cerebrum, including frontal, parietal, temporal lobe, and limbic systems (T = 5.5513, $p < 0.05$ corrected by permutation test with TFCE, absolute ES = 0.34). In addition, subtype 2 were older (T = 4.115, $p < 0.001$) and had higher possibility of hypertension ($\chi^2 = 7.614$, $p = 0.006$) and drinking habbit ($\chi^2 = 4.681$, $p = 0.031$) compared with healthy controls.

Subtype 3 (n = 41) demonstrated widespread abnormalities in CBF compared with healthy subjects (n = 53). Specifically, subtype 3 demonstrated decreased CBF mainly in the posterior part of the brain (occipital, parietal and part of temporal lobe) and bilateral cerebrum (T = 8.1432, $p < 0.05$ corrected by permutation test with TFCE, absolute ES = 0.74). Subtype 3 demonstrated increased CBF in the anterior part of the brain, including the frontal and temporal lobe (T = 6.8409, $p < 0.05$ corrected by permutation test with TFCE, absolute ES = 0.52). Compared with healthy subjects, subtype 3 showed significant differences in age (T = -2.381, $p = 0.019$), gender ($\chi^2 = 6.438$, $p = 0.011$), the proportions of subject with hypertension ($\chi^2 = 7.614$, $p = 0.006$), smoking ($\chi^2 = 9.707$, $p = 0.002$) and drinking habits ($\chi^2 = 11.025$, $p = 0.001$).

Differences in the proportions of patients with MRI markers among three CSVD subtypes are shown in Table 2. Notably, the three subtypes differed in the proportions of patients with lacunes ($p = 0.002$), periventricular WMH (PVWMH) ($p = 0.043$) and total CSVD burden score ($p = 0.048$). Specifically, subtype 1 differed from subtype 2 and subtype 3 in terms of the proportions of patients with lacunes and PVWMH.

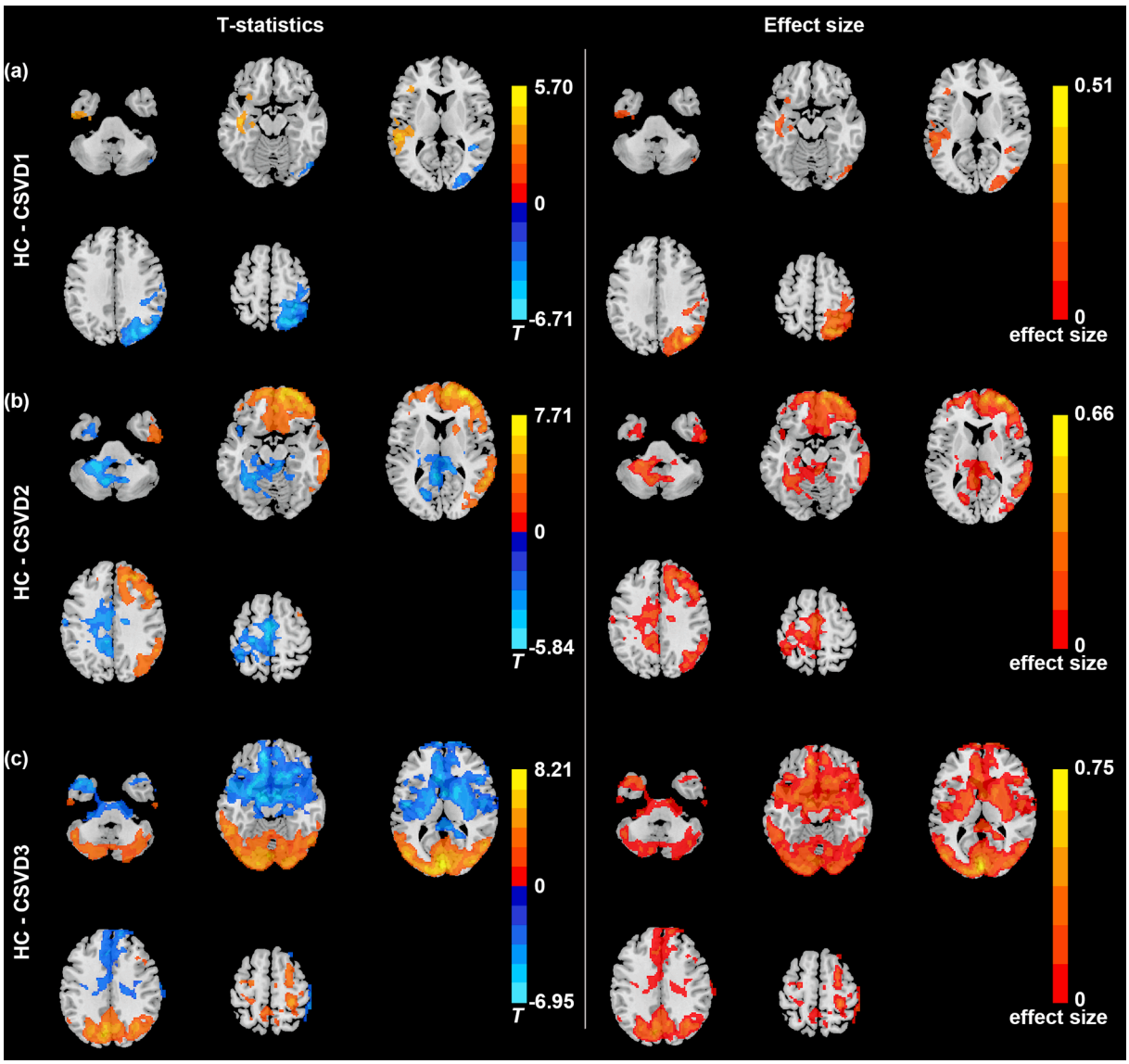

Fig. 2. Patterns of CBF identifying the three CSVD subtypes in comparison with healthy controls. Comparison of CBF map between healthy controls and (a) CSVD subtype 1, (b) CSVD subtype 2, (c) CSVD subtype 3, and corresponding absolute effect size map.

Subtype 3 patients showed higher total burden than subtype 1.

3.4. Correlation analysis

Correlation analysis revealed that within each CSVD subtype, mean CBF of brain regions with decreased CBF was negatively correlated with mean CBF of brain regions with increased CBF (r = -0.629, $p < 0.001$ for subtype 1, r = -0.813, $p < 0.001$ for subtype 2, and r = -0.875, $p < 0.001$ for subtype 3). In addition, CBF of brain regions with decreased CBF was negatively correlated with total CSVD burden score in subtype 3 ($r = -0.324$, $p = 0.029$) (Fig. 3). However, no significant correlations were observed between CBF and total CSVD burden score in the other two subtypes ($r = -0.260$, $p = 0.111$ for subtype 1, and $r = -0.016$, $p = 0.923$ for subtype 2).

3.5. Gray and white matter volumetric differences

By group analysis between healthy controls and CSVD subtypes, we discovered that the three subtypes did not differ in volumetric gray matter patterns. In terms of white matter volumetric differences, CSVD subtype 1 exhibited decreased white matter volume in the bilateral retrosubicular area and right corpus callosum. CSVD subtype 2 showed reduced white matter volume mainly in the right cerebrum, which was consistent with decreased CBF. CSVD subtype 3 experienced widespread white matter volume reduction in the bilateral cerebrum compared with healthy controls (Supplementary Figure S8).

4. Discussion

In this study, via a novel semi-supervised clustering approach, we identified three subtypes of CSVD with distinct CBF patterns. In addition, the three subtypes also demonstrated differences in clinical measures, MRI markers and white matter volumetric patterns. The overall findings of this study are summarized in Fig. 4.

Cerebral small vessels including small arteries, arterioles, venules and capillaries are vital for maintaining the cerebral blood flow (Ashby and Mack, 2021). Therefore, dysfunctions of cerebral small vessels by CSVD leads to the alterations of CBF (Wardlaw et al., 2013). Plausible pathological mechanism is the impairment of brain blood barrier (BBB) (Wong et al., 2019). Both BBB permeability and CBF regulation are functional elements controlled in the neurovascular unit (Stanimirovic and Friedman, 2012). The impairment of BBB, whether due to the

Table 2
MRI markers for different CSVD subtypes.

MRI markers	CSVD 1 (n = 39)	CSVD 2 (n = 41)	CSVD 3 (n = 41)	Statistics	p
Lacunes	5Y/34 N	19Y/22 N	19Y/22 N	$\chi^2 = 12.964$	**0.002**[†]
White matter lesions	15Y/24 N	23Y/18 N	21Y/20 N	$\chi^2 = 2.638$	0.267
PVWMH	6Y/33 N	15Y/26 N	16Y/25 N	$\chi^2 = 6.316$	**0.043**[‡]
DWMH	13Y/26 N	16Y/25 N	10Y/31 N	$\chi^2 = 2.042$	0.360
Total WMH score[**]	0.4872 ± 0.6833	0.7805 ± 0.7910	0.6341 ± 0.6617	$KW = 2.802$	0.246
EVPS in the basal ganglia	34Y/5N	33Y/8N	37Y/4N	$\chi^2 = 1.688$	0.430
EVPS in the centrum semiovale	30Y/9N	36Y/5N	35Y/6N	$\chi^2 = 1.877$	0.391
Total EVPS score[**]	1.6410 ± 0.6277	1.6829 ± 0.6099	1.7561 ± 0.5376	$KW = 0.839$	0.657
CMB	10Y/29 N	12Y/29 N	14Y/27 N	$\chi^2 = 0.699$	0.705
CMB (≤5)	7Y/32 N	10Y/31 N	11Y/30 N	$\chi^2 = 0.941$	0.625
CMB (>5)	3Y/36 N	2Y/39 N	5Y/36 N	$\chi^2 = 1.473$	0.479
Total CMB score[**]	0.3333 ± 0.6213	0.3415 ± 0.5749	0.4878 ± 0.7114	$KW = 1.327$	0.515
CSVD total burden[**]	1.64 ± 0.81	2.12 ± 1.12	2.22 ± 1.11	$KW = 6.063$	**0.048**[§]

[†] CSVD1 vs CSVD2, $\chi^2 = 10.695$, p = 0.001; CSVD1 vs CSVD3, $\chi^2 = 10.695$, p = 0.001.
[‡] CSVD1 vs CSVD2, $\chi^2 = 4.641$, p = 0.031; CSVD1 vs CSVD3, $\chi^2 = 5.602$, p = 0.018.
[§] CSVD1 vs CSVD3, U = 568.5, p = 0.018.
[**]Scores are rated according to the criterion listed in Supplementary Table S1.
Abbreviations: PVWMH, periventricular WMH; DWMH, deep WMH; Y, yes; N, no; CSVD1, CSVD subtype 1; CSVD2, CSVD subtype 2; CSVD3, CSVD subtype 3.

change of basal plate, the injury of endothelia cells or astrocytes, is a common term of many neurodegenerative diseases involving microcirculation pathology (Erdener and Dalkara, 2019).

However, previous findings in relation to the alterations of CBF in CSVD patients were highly inconsistent (Shi et al., 2016; Stewart et al., 2021). The heterogeneity of BBB permeability might account for the inconsistent perfusion patterns to some extent (Rajani et al., 2019). Variances of MRI imaging features including WMH, lacune, CMBs, and EPVS among individuals may also account for the inconsistent perfusion patterns (Wang et al., 2021). In addition, risk factors including hypertension, smoking and drinking may influence brain perfusion (Yu et al., 2020). The above factors highlight the complex hemodynamics of CBF in the CSVD patients and lie foundation of CBF heterogeneity in CSVD patients.

In order to overcome the high heterogeneity of CBF in CSVD patients, we used a novel semi-supervised machine learning method named HYDRA. HYDRA develops a novel non-linear learning algorithm for integrated binary classification and subpopulation clustering, and it uniquely excavates cluster illness effects by modelling differences from healthy controls instead of clustering patients directly (Varol et al., 2017). Unsupervised clustering algorithms like k-means clustering cluster patients according to their similarity, which are easy to confound inter-individual diversity and variability irrelevant to the disease (Varol et al., 2017; Chand et al., 2020). On the contrary, HYDRA can identify inherent disease subtypes by removing the influence of confounding variations introduced by age, gender, scanner, and other factors, and can effectively find the optimal number of subtypes by varying the number of hyperplanes (Varol et al., 2017). In addition, the present three subtypes with distinct CBF patterns clustered by HYDRA were robust to different feature definition strategies, and permutation test against null hypothesis, which proved that the current subtypes had high reproducibility.

A consensus has formed that CSVD is associated with reduced CBF (Wardlaw et al., 2013). However, recent meta-analyses which reviewed cross-sectional studies have questioned the simple relationship between CSVD and CBF (Shi et al., 2016; Stewart et al., 2021). The current study clarified that although reduced CBF was associated with all three subtypes of CSVD patients, the three subtypes of CSVD also exhibited increased CBF in certain brain regions. A previous meta-analysis has found large heterogeneity of CBF in the temporal lobe in CSVD patients (Shi et al., 2016), which was supported by the present findings. Here, we found that decreased CBF in the temporal lobe only occurs in a proportion of CSVD patients (CSVD subtype 1, about 32 % in this study). In subtype 1, the increased CBF was consistent with a study reporting higher CBF with white matter diseases (Kraut et al., 2008). Previous meta-analysis has also demonstrated the least heterogeneity of brain perfusion in the occipital lobe as relevant studies have found more decreased patterns than increased patterns of CBF in the occipital lobe (Shi et al., 2016; Fu et al., 2014). In line with previous findings, the current results revealed that both subtype 2 and 3 exhibited decreased CBF in the occipital lobe, only subtype 1 demonstrated a slight increasing of CBF in the right occipital lobe. Furthermore, relevant studies have reported conflicting results of the CBF in the frontal and parietal regions in CSVD (Fu et al., 2014; Kuwabara et al., 1996), which was in accord with different perfusion patterns in the three CSVD subtypes in this study. A previous study has observed abnormally higher CBF in several brain regions including the right inferior temporal gyrus, right fusiform gyri, right anterior cingulate, left superior temporal gyrus, and left middle temporal gyrus (Kraut et al., 2008). The present findings regarding CSVD alterations in CSVD subtype 1 and subtype 2 could give the abnormal increasing of CBF a possible explanation. It was also worth mentioning that CSVD subtype 3 exhibited decreased CBF in the posterior part of the brain (the territory of vertebral artery and basilar-artery), and increased CBF in the anterior part of the brain (the territory of carotid artery), indicating that cerebral hypoperfusion of CSVD subtype 3 might originate from bilateral vertebral arteries insufficiency.

Traditional studies of CSVD have been conducted before determining subtypes on the basis of perfusion patterns, these studies commonly revealed overlapping relationships between CSVD clinical symptoms and CBF (Chen et al., 2021; Jann et al., 2021; Yu et al., 2020). In the current study, associations between clinical symptoms and CSVD were assessed after determining the CSVD subtypes, and several common risk factors between healthy controls and CSVD patients were found, including age, proportion of subjects drinking alcohol. In addition, healthy controls and some subtypes of CSVD patients differed in the proportion of subjects having hypertension and smoking cigarette. Ageing is a common risk factor for cerebral vascular diseases due to the fact that cerebral microvasculature is exceptionally vulnerable to changes due to ageing (Shaaban et al., 2019). Previous studies found associations between age and decreased CBF (Chen et al., 2011; Yu et al., 2020). Hypertension, smoking cigarette, drinking alcohol are also common risk factors for CSVD clinically as several studies have found associations between these risk factors and CSVD severity (Cannistraro et al., 2019; Moniruzzaman et al., 2020). However, we found that only drinking alcohol is a risk factor for all CSVD patients, while hypertension and smoking cigarette are risk factors for certain CSVD subtypes. In addition, we found that healthy controls and different CSVD subtypes differed in gender ratios, furthermore, the three different subtypes differed in gender ratios. Gender-related alterations in CBF have been reported in the healthy (Chen et al., 2011). Ambarki et al. have demonstrated that females tend to have higher CBF values than males (Ambarki et al., 2015). Therefore, it was supposed that the differences in gender might contribute to the heterogeneity of CSVD.

Among the three CSVD subtypes observed in the present study, subtype 2 and 3 patients experience higher possibility of lacunes and PVWMH compared with subtype 1. Lacunes and WMH are two common MRI markers of CSVD patients (Xin et al., 2019). Zhang et al. have reported that an increased pericarotid fat density is associated with the presence of lacunes, and may be linked to CSVD (Zhang et al., 2021). A previous cross-sectional study has provided evidence which linked lacunes and WMHs to a common pathogenesis of CSVD (Yu et al., 2021).

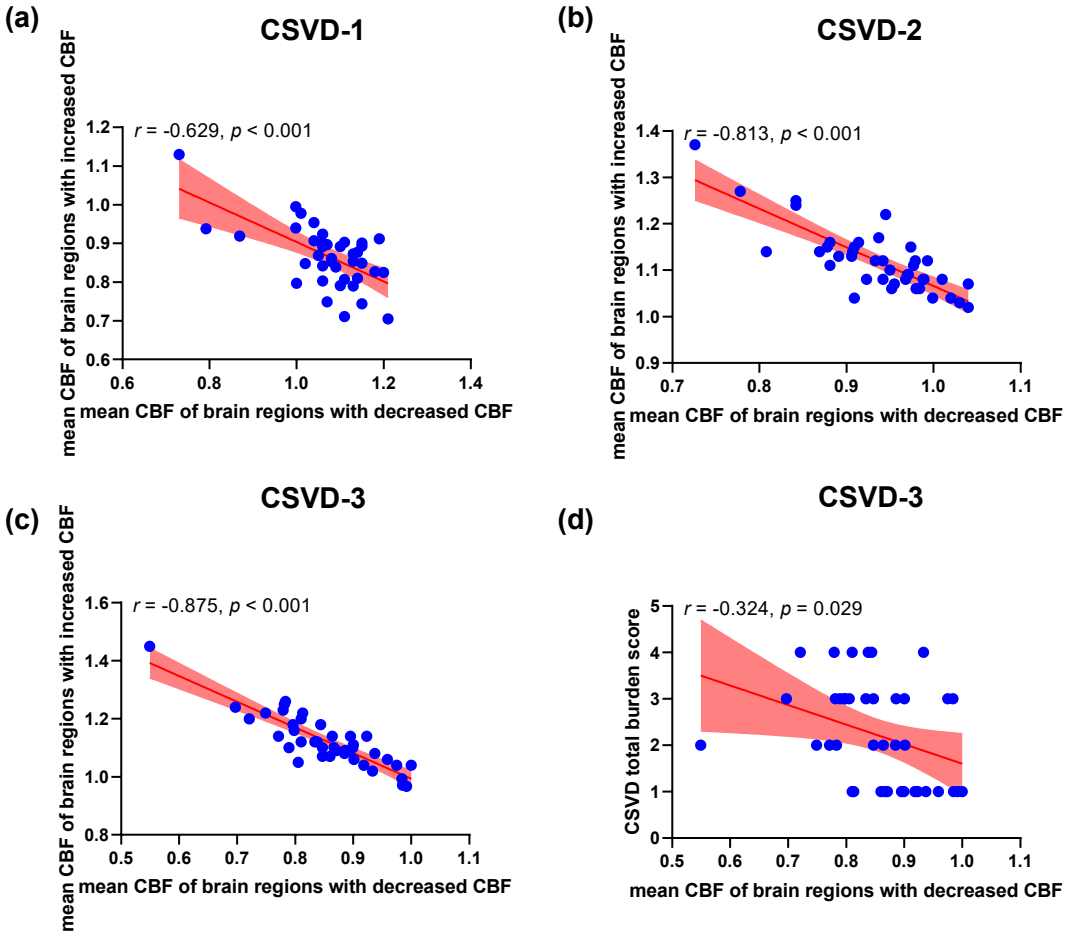

Fig. 3. Associations between CBF and clinical measures in the three CSVD subtypes. (a) CBF in the regions with decreased CBF compared with healthy controls (HCs) is negatively associated with CBF in the regions with increased CBF compared with HCs in (a) subtype 1, (b) subtype 2, (c) subtype 3. (d) CBF in the regions with decreased CBF compared with HCs is negatively associated with total CSVD burden score in subtype 3. The light red regions indicate 95% confidence interval.

In addition, CSVD subtype 2 and subtype 3 also showed higher possibility of PVWMH but not deep WMH (DWMH) compared with subtype 1. Both cross-sectional and longitudinal studies have demonstrated that decreased CBF was related to PVWMH rather than DWMH (Promjunyakul et al., 2018; ten Dam et al., 2007), which was consistent with our findings. However, whether the development of PVWMH and DWMH differs in mechanisms still remain unanswered. In short, the three subtypes of CSVD differed in the possibility of lacunes and PVWMH, and lacunes and PVWMH were two critical markers contributing to the severity of CSVD since subtype 2 and 3 showed wider alterations of CBF, and higher total burden score compared with subtype 1.

All the three subtypes of CSVD showed plausible compensatory phenomenon in cerebral perfusions. The dynamics of regional CBF are complex and regionally specific. The decreased CBF across the three CSVD subtype resulted in reduced resting cerebral cortical activity. However, the brain needs to maintain the cortical activity, which would require increased blood flow to balance the metabolic demands (Kraut et al., 2008). Therefore, each subtype showed both increased and decreased CBF across the entire brain, and significant associations between perfusions in brain regions with increased and decreased CBF were observed across all three subtypes. In addition, only within CSVD subtype 3, total burden score was negatively correlated with CBF, which was in contradiction with previous results (Yu et al., 2020). The inconsistent result may be due to the fact that total CSVD burden score is a general indicator of the disease (Yu et al., 2020). However, some markers such as lacunes and WMH may contribute more to the alterations of CBF, while other markers may play limited roles in CBF changes. In this sense, the association between total CSVD burden score and CBF alterations may be weakened.

CSVD is characterized by progressive cerebral white matter changes due to chronic low perfusion and loss of autoregulation (Han et al., 2019). In the current study, voxel-wise comparisons of gray and white matter volumes demonstrated less gray matter volume alterations, but more white matter volume reductions in CSVD, which was consistent with the previous consensus that CSVD was associated with white matter abnormalities (Liu et al., 2020; Wang et al., 2021). In addition, subtype 2 and subtype 3 experienced similar patterns of white matter volume loss, but exhibited distinct patterns of cerebral circulation, which highlighted the heterogeneity of cerebral perfusion in CSVD.

The three subtypes of the current study may further contribute to individualized treatment of CSVD in the future. Recently, photobiomodulation therapies such as red to near-infrared light treatment have been shown as efficient methods for disorders such as stroke and brain trauma, which can help the brain repair itself by stimulating neurogenesis, upregulating BDNF synthesis, and encouraging synaptogenesis (Iglesias-Rey and Castillo, 2020). Irradiation location is a critical factor for the photobiomodulation therapies (Salehpour et al., 2018). So far, several approaches including transcranial photobiomodulation therapy, intranasal photobiomodulation therapy, brain photobiomodulation via oral cavity have been proposed to delivery light to different parts of the brain (Hamblin, 2018). These therapies targeting to specific brain regions of each subtype identified by the current results may enhance the therapeutic effect of CSVD. In addition, the three subtypes of CSVD differs in clinical profiles. Therefore, controlling

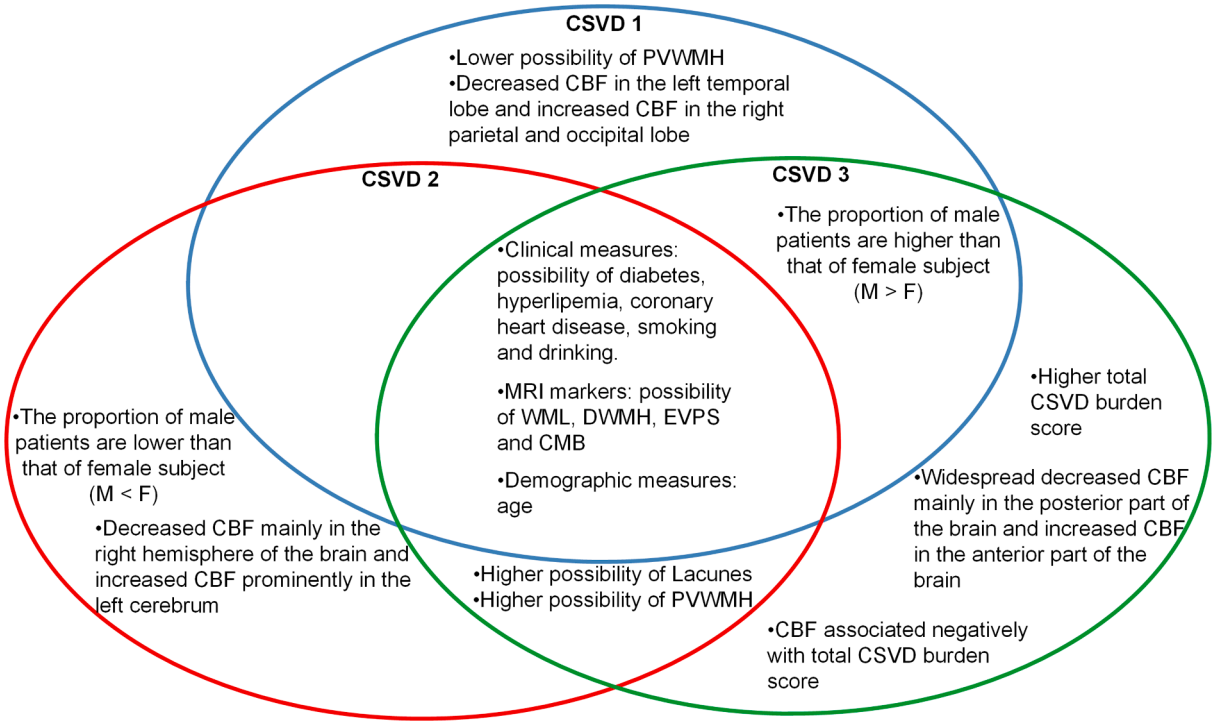

Fig. 4. Summary of the three CSVD subtypes.

relevant clinical profiles may be beneficial to certain subtypes. For instance, controlling blood pressure may be more effective to subtype 2 and 3, smoking cessation may be more beneficial to subtype 1 and 3.

The present findings suggest several challenges for future research. Firstly, the three subtypes of CSVD may exhibit different perfusion trajectories over time, which may further lead to differences in clinical and imaging manifestations including hypertension, lacunes, WMHs. However, due to the cross-sectional nature of the current study, differences in longitudinal trajectories cannot be assessed. Longitudinal data are needed to address how CBF changes over time and relates to changes in clinical phenotypes over time in different CSVD subtypes. Secondly, the moderate sample size may weaken the interpretation of the current findings. A larger sample with the current approach might result in a different clustering solution, which should be a main focus in the future. Thirdly, due to limited conditions, clinical measures including hypertension, smoking, drinking were all binary, which may hinder the clinical interpretation. Future studies should pay attention to the collection of clinical information.

5. Conclusion

In summary, we uncovered three markedly distinct perfusion subtypes of CSVD. Subtype 1 showed decreased CBF in the left temporal lobe and increased CBF in the right parietal lobe, right precuneus, right postcentral gyrus, and right occipital lobe. Subtype 2 exhibited reduced CBF in the right hemisphere of the brain, and increased CBF in the left cerebrum. While subtype 3 demonstrated decreased CBF in the brain posterior regions and increased CBF in the brain anterior regions. The three subtypes of CSVD patients also differed in terms of gender, total CSVD burden, proportions of subjects with lacunes, PVWMH and whiter matter patterns. The three subtypes demonstrated differences in the associations between CBF and clinical measures, which could contribute to the understanding of CSVD pathology, and also to the precision clinical care that accounts for the biological heterogeneity in the diagnosis and treatment of CSVD.

Data availability statement

The data that support the findings of this study are available from the corresponding author upon reasonable request.

Funding

This study was supported by the Taishan Scholars Program of Shandong Province (Grant No: TS201712065), Academic Promotion Program of Shandong First Medical University (Grant number: 2019QL009), and Science and Technology funding from Jinan (Grant number: 2020GXRC018).

CRediT authorship contribution statement

Weizhao Lu: Formal analysis, Methodology, Software, Writing – original draft, Writing – review & editing. **Chunyan Yu:** Data curation, Resources, Validation, Visualization. **Liru Wang:** Data curation, Resources, Validation, Visualization. **Feng Wang:** Conceptualization, Data curation, Resources, Supervision, Writing – review & editing. **Jianfeng Qiu:** Conceptualization, Funding acquisition, Supervision, Writing – review & editing.

Declaration of Competing Interest

The authors declare that they have no known competing financial interests or personal relationships that could have appeared to influence the work reported in this paper.

Data availability

Data will be made available on request.

Appendix A. Supplementary data

Supplementary data to this article can be found online at https://doi.org/10.1016/j.nicl.2022.103165.

References

Ambarki, K., Wåhlin, A., Zarrinkoob, L., et al., 2015. Accuracy of parenchymal cerebral blood flow measurements using pseudocontinuous arterial spin-labeling in healthy volunteers. Am. J. Neuroradiol. 36, 1816–1821.

Ashby, J.W., Mack, J.J., 2021. Endothelial control of cerebral blood flow. Am. J. Pathol. (21) S0002-9440(21)00103-6.

Binnie, L.R., Pauls, M.M.H., Benjamin, P., et al., 2022. Test-retest reliability of arterial spin labelling for cerebral blood flow in older adults with small vessel disease. Transl Stroke Res.

Cannistraro, R.J., Badi, M., Eidelman, B.H., et al., 2019. CNS small vessel disease: a clinical review. Neurology 92, 1146–1156.

Chand, G.B., Dwyer, D.B., Erus, G., et al., 2020. Two distinct neuroanatomical subtypes of schizophrenia revealed using machine learning. Brain 143, 1027–1038.

Chen, J.J., Rosas, H.D., Salat, D.H., 2011. Age-associated reductions in cerebral blood flow are independent from regional atrophy. Neuroimage 55, 468–478.

Chen, X., Wang, J., Shan, Y., et al., 2019. Cerebral small vessel disease: neuroimaging markers and clinical implication. J. Neurol. 266, 2347–2362.

Chen, X., Lu, D., Guo, N., et al., 2021. Left ventricular ejection fraction and right atrial diameter are associated with deep regional CBF in arteriosclerotic cerebral small vessel disease. BMC Neurol. 21, 67.

Erdener, Ş.E., Dalkara, T., 2019. Small vessels are a big problem in neurodegeneration and neuroprotection. Front. Neurol. 10, 889.

Fan, L., Li, H., Zhuo, J., et al., 2016. The human brainnetome atlas: a new brain atlas based on connectional architecture. Cereb Cortex. 26, 3508–3526.

Fu, J., Tang, J., Han, J., Hong, Z., 2014. The reduction of regional cerebral blood flow in normal-appearing white matter is associated with the severity of white matter lesions in elderly: a Xeon-CT study. PLoS ONE 9, e112832.

Hamblin, M.R., 2018. Photobiomodulation for traumatic brain injury and stroke. J. Neurosci. Res. 96, 731–743.

Han, H.J., Kim, B.C., Youn, Y.C., et al., 2019. A comparison study of cilostazol and aspirin on changes in volume of cerebral small vessel disease white matter changes: protocol of a multicenter, Randomized Controlled Trial. Dement. Neurocogn. Disord. 18, 138–148.

Hillis, A.E., Wityk, R.J., Barker, P.B., et al., 2002. Subcortical aphasia and neglect in acute stroke: the role of cortical hypoperfusion. Brain 125, 1094–1104.

Iglesias-Rey R, Castillo J. New strategies for ischemic stroke: internal photobiomodulation therapy. Neural Regen. Res. 2020;15:1658-1659.

Jann, K., Shao, X., Ma, S.J., et al., 2021. Evaluation of cerebral blood flow measured by 3D PCASL as biomarker of vascular cognitive impairment and dementia (VCID) in a cohort of elderly latinx subjects at risk of small vessel disease. Front Neurosci. 15, 627627.

Kraut, M.A., Beason-Held, L.L., Elkins, W.D., Resnick, S.M., 2008. The impact of magnetic resonance imaging-detected white matter hyperintensities on longitudinal changes in regional cerebral blood flow. J. Cereb. Blood Flow Metab. 28, 190–197.

Kuwabara, Y., Ichiya, Y., Sasaki, M., et al., 1996. Cerebral blood flow and vascular response to hypercapnia in hypertensive patients with leukoaraiosis. Ann. Nucl. Med. 10, 293–298.

Lawrence, A.J., Chung, A.W., Morris, R.G., Markus, H.S., Barrick, T.R., 2014. Structural network efficiency is associated with cognitive impairment in small-vessel disease. Neurology 83, 304–311.

Li, Q., Yang, Y., Reis, C., et al., 2018. Cerebral small vessel disease. Cell Transplant. 27, 1711–1722.

Liu, C., Zou, L., Tang, X., et al., 2020. Changes of white matter integrity and structural network connectivity in nondemented cerebral small-vessel disease. J. Magn. Reson. Imaging. 51, 1162–1169.

Moniruzzaman, M., Kadota, A., Segawa, H., et al., 2020. Relationship between step counts and cerebral small vessel disease in Japanese Men. Stroke 51, 3584–3591.

Pantoni, L., 2010. Cerebral small vessel disease: from pathogenesis and clinical characteristics to therapeutic challenges. Lancet Neurol. 9, 689–701.

Promjunyakul, N.O., Dodge, H.H., Lahna, D., et al., 2018. Baseline NAWM structural integrity and CBF predict periventricular WMH expansion over time. Neurology 90, e2119–e2126.

Rajani, R.M., Ratelade, J., Domenga-Denier, V., et al., 2019. Blood brain barrier leakage is not a consistent feature of white matter lesions in CADASIL. Acta Neuropathol. Commun. 7 (1), 187.

Rolls, E.T., Huang, C.C., Lin, C.P., Feng, J., Joliot, M., 2020. Automated anatomical labelling atlas 3. Neuroimage. 206, 116189.

Salehpour, F., Mahmoudi, J., Kamari, F., Sadigh-Eteghad, S., Rasta, S.H., Hamblin, M.R., 2018. Brain photobiomodulation therapy: a narrative review. Mol Neurobiol. 55, 6601–6636.

Salvadori, E., Poggesi, A., Valenti, R., et al., 2016. Operationalizing mild cognitive impairment criteria in small vessel disease: the VMCI-Tuscany Study. Alzheimers Dement. 12, 407–418.

Shaaban, C.E., Jorgensen, D.R., Gianaros, P.J., Mettenburg, J., Rosano, C., 2019. Cerebrovascular disease: Neuroimaging of cerebral small vessel disease. Prog. Mol. Biol. Transl. Sci. 165, 225–255.

Shi, Y., Thrippleton, M.J., Makin, S.D., et al., 2016. Cerebral blood flow in small vessel disease: A systematic review and meta-analysis. J. Cereb. Blood Flow Metab. 36, 1653–1667.

Shi, Y., Wardlaw, J.M., 2016. Update on cerebral small vessel disease: a dynamic whole-brain disease. Stroke Vasc. Neurol. 1, 83–92.

Spreng, R.N., Sepulcre, J., Turner, G.R., Stevens, W.D., Schacter, D.L., 2013. Intrinsic architecture underlying the relations among the default, dorsal attention, and frontoparietal control networks of the human brain. J. Cogn. Neurosci. 25, 74–86.

Stanimirovic, D.B., Friedman, A., 2012. Pathophysiology of the neurovascular unit: disease cause or consequence? J. Cereb. Blood Flow Metab. 32, 1207–1221.

Stewart, C.R., Stringer, M.S., Shi, Y., Thrippleton, M.J., Wardlaw, J.M., 2021. Associations between white matter hyperintensity burden, cerebral blood flow and transit time in small vessel disease: an updated meta-analysis. Front. Neurol. 12, 647848.

ten Dam, V.H., van den Heuvel, D.M., de Craen, A.J., et al., 2007. Decline in total cerebral blood flow is linked with increase in periventricular but not deep white matter hyperintensities. Radiology 243, 198–203.

Ter Telgte, A., van Leijsen, E.M.C., Wiegertjes, K., et al., 2018. Cerebral small vessel disease: from a focal to a global perspective. Nat. Rev. Neurol. 14, 387–398.

Tuladhar, A.M., Lawrence, A., Norris, D.G., et al., 2017. Disruption of rich club organisation in cerebral small vessel disease. Hum Brain Mapp. 38, 1751–1766.

Tullberg, M., Fletcher, E., DeCarli, C., et al., 2004. White matter lesions impair frontal lobe function regardless of their location. Neurology 63, 246–253.

Varol, E., Sotiras, A., Davatzikos, C., 2017. Alzheimer's disease neuroimaging initiative. HYDRA: revealing heterogeneity of imaging and genetic patterns through a multiple max-margin discriminative analysis framework. Neuroimage 145, 346–364.

Wang, T., Jin, A., Fu, Y., Zhang, Z., Li, S., Wang, D., Wang, Y., 2021. Heterogeneity of white matter hyperintensities in cognitively impaired patients with cerebral small vessel disease. Front Immunol. 12, 803504.

Wang, Q., Su, N., Huang, J., et al., 2021. White matter but not gray matter volumes are associated with cognition in community-dwelling chinese populations. J. Alzheimers Dis. 84, 367–375.

Wardlaw, J.M., Smith, E.E., Biessels, G.J., et al., 2013. Neuroimaging standards for research into small vessel disease and its contribution to ageing and neurodegeneration. Lancet Neurol. 12, 822–838.

Wardlaw, J.M., Benveniste, H., Nedergaard, M., et al., 2020. Perivascular spaces in the brain: anatomy, physiology and pathology. Nat. Rev. Neurol. 16, 137–153.

Wong, S.M., Jansen, J.F.A., Zhang, C.E., et al., 2019. Blood-brain barrier impairment and hypoperfusion are linked in cerebral small vessel disease. Neurology 92, e1669–e1677.

Xin, J., Huang, X., Pan, X., et al., 2019. Risk factors for aphasia in cerebral small vessel diseases. Curr. Neurovasc. Res. 16, 107–114.

Yu, C., Lu, W., Qiu, J., Wang, F., Li, J., Wang, L., 2020. Alterations of the whole cerebral blood flow in patients with different total cerebral small vessel disease burden. Front. Aging Neurosci. 12, 175.

Yu, X., Yin, X., Hong, H., et al., 2021. Increased extracellular fluid is associated with white matter fiber degeneration in CADASIL: in vivo evidence from diffusion magnetic resonance imaging. Fluids Barriers CNS. 18, 29.

Zhang, D.H., Jin, J.L., Zhu, C.F., Chen, Q.Y., He, X.W., 2021. Association between carotid artery perivascular fat density and cerebral small vessel disease. Aging 13, 18839–18851.

Zilles, K., Amunts, K., 2010. Centenary of Brodmann's map–conception and fate. Nat. Rev. Neurosci. 11, 139–145.